ADVANCING EARTH AND SPACE SCIENCES

JGR Atmospheres

RESEARCH ARTICLE
10.1029/2025JD043492

Multidecadal Variability in Atmospheric Dust Preserved in an Ice Core From the Southern Slopes of the Himalayas

Nao Esashi[1], Akane Tsushima[2], Sumito Matoba[3], Yoshinori Iizuka[3], Ryu Uemura[1], Rijan B. Kayastha[4], and Koji Fujita[1]

[1]Graduate School of Environmental Studies, Nagoya University, Nagoya, Japan, [2]Graduate School of Integrated Science and Technology, Nagasaki University, Nagasaki, Japan, [3]Institute of Low Temperature Science, Hokkaido University, Sapporo, Japan, [4]Himalayan Cryosphere, Climate and Disaster Research Center, Department of Environmental Science and Engineering, School of Science, Kathmandu University, Dhulikhel, Nepal

Key Points:

- A 145-year record of atmospheric dust was reconstructed from an 81.2-m-long ice core drilled on the southern slopes of the Himalayas
- Differences in dust concentration and particle size between northern and southern slopes of the Himalayas were studied
- Dust concentrations exhibit variability synchronized with Atlantic Multidecadal Oscillation reflecting surface condition of dust sources

Correspondence to:
N. Esashi,
nao.esashi@gmail.com

Citation:
Esashi, N., Tsushima, A., Matoba, S., Iizuka, Y., Uemura, R., Kayastha, R. B., & Fujita, K. (2025). Multidecadal variability in atmospheric dust preserved in an ice core from the southern slopes of the Himalayas. *Journal of Geophysical Research: Atmospheres*, *130*, e2025JD043492. https://doi.org/10.1029/2025JD043492

Received 24 JAN 2025
Accepted 28 MAY 2025

Author Contributions:
Conceptualization: Akane Tsushima, Koji Fujita
Data curation: Nao Esashi, Akane Tsushima, Sumito Matoba, Yoshinori Iizuka
Formal analysis: Nao Esashi, Koji Fujita
Funding acquisition: Koji Fujita
Investigation: Nao Esashi, Akane Tsushima, Rijan B. Kayastha, Koji Fujita
Methodology: Nao Esashi, Koji Fujita
Project administration: Rijan B. Kayastha, Koji Fujita
Visualization: Nao Esashi, Koji Fujita
Writing – original draft: Nao Esashi, Koji Fujita
Writing – review & editing: Sumito Matoba, Yoshinori Iizuka, Ryu Uemura

Abstract Ice cores from the Himalayan region, downwind from vast arid and densely populated areas, are important in revealing long-term dust variability and the driving factors behind such variability. However, logistical challenges in reaching the region have hindered the retrieval of long-term dust records from the southern side of the Himalayas. This study presents a 145-year record of atmospheric dust from an 81.2-m ice core drilled in the Trambau (TB) glacier, a south-facing glacier in the Nepal Himalaya, covering 1875–2019 CE. Comparison of dust records from the northern and southern slopes of the Himalayas indicates that the ice core from the southern slopes has preserved higher dust concentrations and larger particle sizes than records from the northern slopes. Furthermore, the TB core record shows 50- to 70-year multidecadal variability, positively correlated with the Atlantic Multidecadal Oscillation (AMO). Based on correlation and composite analyses using ERA5 reanalysis data, AMO phases have been linked with surface wetness/dryness in dust source regions in the Middle East and Southwest Asia, likely contributing to variations in dust loading at the TB core site.

Plain Language Summary The Himalayan range acts as a significant barrier to atmospheric flow, influencing dust transport and deposition patterns. Ice cores from this region provide critical insights into how atmospheric dust levels have changed over time, and the factors driving these changes. However, the challenging terrain has limited the collection of long-term records, especially from the southern side of the Himalayas. We analyzed an 81.2-m-long ice core drilled in the Trambau glacier on the southern slopes of the Nepal Himalayas, spanning the period 1875–2019 CE. The southern slopes have higher dust concentrations and larger particle sizes than the northern slopes. Moreover, dust levels show a 50- to 70-year variability linked to the Atlantic Multidecadal Oscillation (AMO). AMO phases are connected to wet or dry conditions in dust source regions such as the Middle East, influencing dust transport to the glacier site.

1. Introduction

Dust aerosols have widespread effects on climate, biogeochemical and hydrological cycles, and human health. Earth's radiative balance and thus surface and air temperatures are affected by aerosol scattering and absorption of incoming solar radiation and re-emission of outgoing longwave radiation (Ji et al., 2016; Miller & Tegen, 1998). Cloud properties and precipitation patterns are affected by dust aerosols (Rosenfeld et al., 2001), and essential nutrients such as iron are supplied to the oceans in dust, boosting marine productivity (Jickells et al., 2005). Finally, fine particles threaten human respiratory health (Griffin & Kellogg, 2004). Given these effects, it is important that the temporospatial variability in atmospheric dust loading, and the relevant driving factors, are understood.

Glaciers in High-Mountain Asia (HMA) are located near or downwind of major dust sources such as the Sahara, Arabian, Taklamakan, and Gobi deserts (Figure 1a; Prospero et al., 2002; Ginoux et al., 2012). Many such glaciers occur in the free troposphere at elevations above 5,000 m, where they receive local material from surrounding rock walls and dust transported from remote arid regions. The concentration and composition of dust deposited on glaciers thus reflect its source and atmospheric conditions during transport, and ice cores provide valuable insights into past climatic and environmental changes (Thompson et al., 1989; Y. Zhang et al., 2015).

Ice cores have been extracted from HMA glaciers, particularly on the Tibetan Plateau and in Central Asia. However, in the Himalayan region, the number of ice cores is limited due to logistical difficulties, and long-term

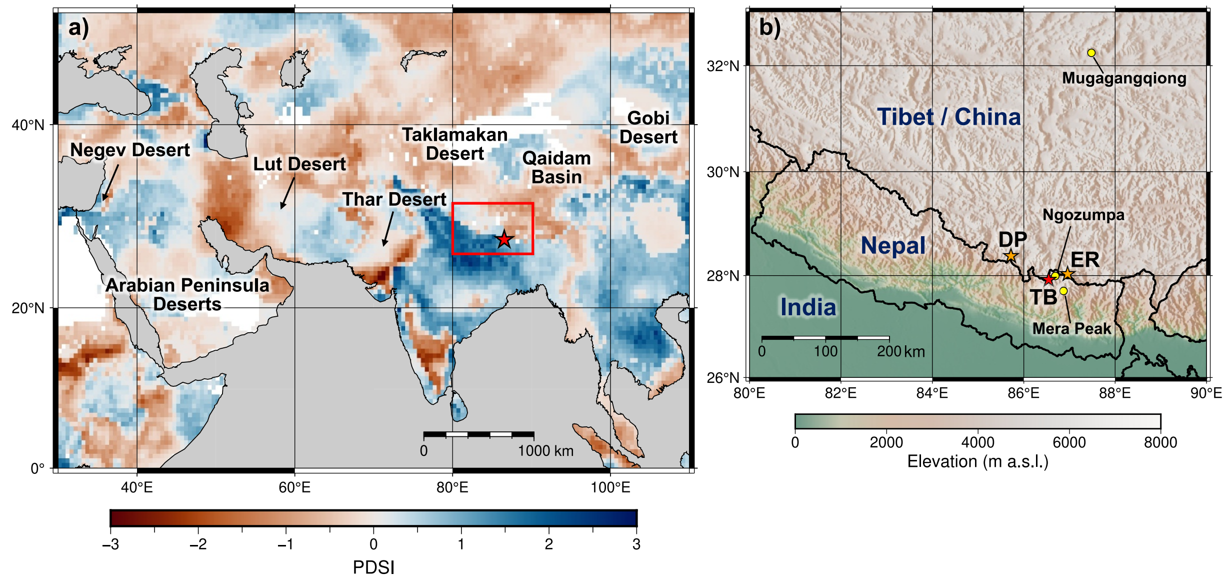

Figure 1. Map of arid regions and the study area. (a) Distribution of Palmer Drought Severity Index averaged for 1901–2022 with arid regions. Negative values indicate dry conditions. The red rectangle marks the area shown in (b). (b) Locations of the three Himalayan ice core sites: Trambau (TB; this study), Dasuopu (DP; Thompson et al., 2000), and East Rongbuk (ER; Xu et al., 2010), and other ice core and snow sampling sites mentioned in the text. The color scale represents elevation (m a.s.l.).

records spanning several centuries have been reconstructed for only two sites: the East Rongbuk glacier (ER core) on Mt. Everest (e.g., Kang et al., 2002; Kaspari et al., 2007; Qin et al., 2002) and the Dasuopu glacier (DP core) on Mt. Shishapangma (Thompson et al., 2000) (Figure 1b). The ER core revealed a positive correlation between dust concentration and reconstructed air temperatures, reflecting cold-humid and warm-dry climatic patterns of dust source regions in Central Asia over the past five centuries (Xu et al., 2010). For the period since the 1950s, dust concentrations in the ER core are negatively correlated with the North Atlantic Oscillation (NAO), suggesting that winter NAO conditions may influence dust storm activity over the Tibetan Plateau (Xu et al., 2007). In contrast, dust concentrations in the DP core indicate the strength of the monsoon, with high-dust events corresponding to historical droughts in India caused by monsoon failure (Thompson et al., 2000). However, these findings are based on ice cores from the northern Himalayan slopes, and north-south differences across the Himalayan range remain unclear.

Extensive studies of snow and ice across the HMA including both the northern and southern slopes of the Himalayas and the Tibetan Plateau have identified the physiographic characteristics of these regions and found that dust concentrations in snow and ice on the southern slopes were relatively low, suggesting a minimal influence of Asian dust, although this conclusion was based on a short-term record limited to the 1990s (Wake et al., 1994). In contrast, a more recent study of a 20-m ice core drilled at Mera Peak on the southern slopes of the Himalayas, covering the 2000s period, revealed remarkably high dust concentrations (Ginot et al., 2014). Dust records for the southern slopes are thus restricted to brief periods of less than a decade, and the results of the few existing studies are not necessarily consistent.

Direct observations of atmospheric aerosols have been conducted at the Nepal Climate Observatory-Pyramid (NCO-P), located at 5,079 m a.s.l. on the southern slope of Mt. Everest (Bonasoni et al., 2010). This region is downwind of the Indo-Gangetic Plain, one of the most densely populated areas in the world, and the observations show strong influence from anthropogenic emissions. Desert dust events are also regularly recorded at NCO-P (Bonasoni et al., 2010; Cristofanelli et al., 2010). However, these records span only the past few years. To investigate how aerosol deposition has changed over more than a century in the southern Himalayas, which are highly sensitive to regional emissions, and to identify its driving forces, ice cores offer essential paleoclimate archives.

This study aimed to establish a new dust record spanning the past 145 years, using an ice core drilled on the southern slopes of the Himalayas, and to clarify the characteristics of atmospheric dust deposition in the region.

Factors controlling decadal-scale variability in dust concentrations were investigated through comparison of this record with neighboring ice core records and climate indices.

2. Methods

2.1. Ice Core Sample and Preprocessing

An 81.2-m ice core (the TB core) was drilled in November 2019 in the Trambau glacier at 5,862 m a.s.l. in the Rolwaling region, eastern Nepal (27.919°N, 86.545°E; Figure 1b; Tsushima et al., 2021). Annual accumulation at the site was estimated to be 730 ± 390 mm water equivalent (w.e.), based on stake measurements and mass-balance simulations (Sunako et al., 2019). The ice core was transported to Japan in a frozen state (Tsushima et al., 2021).

In the cold laboratory at the Institute of Low Temperature Science, Hokkaido University, Japan, the ice core was divided into 1592 sections, each ∼50 mm in length, using a bandsaw. To remove contamination resulting from drilling and transport, the outer surface of each sample was shaved off using a clean ceramic knife in a cold, clean room (Class 10,000). The decontaminated samples were sealed in clean polyethylene bags and melted at ambient temperature. Melted samples were stored in polyethylene bottles for analysis of major ions, pollen, and dust. The ice core was dated by counting peaks of NO_3^- and Ca^{2+} as winter boundaries, revealing that the 81.2-m TB core preserves a 145-year record from 1875 to 2019 CE (Tsushima et al., 2025). For measurements of dust concentrations, small samples (less than ∼3 mL w.e.) were combined, and a total of 1,437 samples from top to bottom of the core were analyzed.

2.2. Dust Analysis

Dust concentrations were determined for the entire core, which contained some large particles of ∼1 mm diameter. However, for Himalayan ice cores, particles of >10 μm diameter are considered to be of local origin, likely sourced from surrounding glacier sediments or rock walls. Such particles constitute <1% of the particle number concentration and have negligible impact on the interpretation of dust concentration data (Xu et al., 2010). These particles were removed by filtration of samples with 10 μm PC membrane filters (Isopore, Merck Millipore, Germany). Solutions for analysis (15 mL) were prepared by mixing 3 mL of sample with 12 mL of diluent (ISOTON II, Beckman Coulter Inc., USA) in 25 mL bottles (Accuvette ST, Beckman Coulter Inc., USA). The mixtures were left to stand for at least 12 hr before analysis, to ensure the dissolution of any air bubbles, and were gently stirred immediately prior to analysis to homogenize any settled particles, with minimum influence of bubbles.

Dust concentrations and particle-size distributions were determined using a Coulter Counter Multisizer 3 (Beckman Coulter Inc., USA) with a 30 μm aperture and counting in 300 channels spanning 0.6–18 μm diameter (on a logarithmic scale). Each concentration value represents the average of at least three independent analyses of the same sample. Uncertainty in repeated measurements averaged ±2.9% for number concentration (range 0.05%–12.5%). Background values were determined through blank tests with ultrapure water (18.2 MΩ cm), with each sample comprising 3 mL ultrapure water and 12 mL diluent. The average blank error in number concentration was 8.6%. As larger particles were removed by filtration, data for particles of 0.6–10 μm diameter only are included here. Dust mass concentration was calculated from the measured dust volume, assuming a spherical approximation and a particle density of 2.5 g cm^{-3} (Delmonte et al., 2002).

2.3. Meteorological and Climate Data

Trends in dust concentrations were compared with climate indices. The NAO is an atmospheric pressure pattern between the Icelandic Low and Azores High (e.g., Luterbacher et al., 2001; Ortega et al., 2015; Yu & Zhou, 2004). The Atlantic Multidecadal Oscillation (AMO) is an index of multidecadal variability of North Atlantic sea surface temperature (SST) (e.g., Delworth & Mann, 2000; Enfield et al., 2001), based on detrended SST anomalies across the North Atlantic region (Wang et al., 2012). In recent years, the term Atlantic Multidecadal Variability has been increasingly used rather than AMO (Birkel et al., 2018; Booth et al., 2012).

Our identification of potential source regions of dust and chemical species preserved in the ice core was based on air-mass Hybrid Single-Particle Lagrangian Integrated Trajectory (HYSPLIT) trajectories distributed by the US National Oceanographic and Atmospheric Administration (Stein et al., 2015). Initial air masses for 10-day back-trajectories were set at 50, 500, 1,000, and 1,500 m above ground level (a.g.l.) at the TB site. The probability distribution of air masses below 1,500 m a.g.l. was calculated at 1° resolution (Iizuka et al., 2018; Parvin et al., 2019).

Correlation and composite analyses were undertaken using the European Center for Medium-range Weather Forecasts (ECMWF) ERA5 reanalysis data set (Hersbach et al., 2020) and the Palmer Drought Severity Index (PDSI, a metric of meteorological drought) (Dai et al., 2004; Palmer, 1965) to investigate the meteorological and surface conditions of potential dust source regions. Composite anomalies of 2-m temperature, 500 hPa wind components, precipitation, and PDSI were considered for the 5 years of most positive AMO (2008, 2009, 2015, 2016, 2017) and most negative AMO (1972, 1973, 1974, 1975, 1976). PDSI data were obtained from the global Climatic Research Unit (CRU, University of East Anglia, UK) at 0.5° resolution (Barichivich et al., 2022; van der Schrier et al., 2013).

Visualization of atmospheric dust loading on a wide spatial scale was based on Aerosol Optical Depth (AOD) data from satellite observations, with AOD quantifying the degree to which dust and other particles in the atmosphere reduce direct sunlight intensity. AOD spatial distributions at 1° resolution were obtained from the Moderate Resolution Imaging Spectroradiometer (MODIS; Prasad & Singh, 2007; Ginoux et al., 2012).

3. Results and Discussion

3.1. Dust Concentration and Size Distribution

Core average (± standard deviation, 1σ) dust number and mass concentrations were $(10.4 \pm 8.0) \times 10^4$ mL^{-1} and $(0.7 \pm 0.6) \times 10^3$ μg kg^{-1}, respectively (Figures 2a and c). The timing of peaks in both number and mass concentration were synchronized, with a strong correlation ($r = 0.92$) of annual means ($p < 0.001$). The proportion of larger particles (>5 μm) averaged 0.6% for number and 25.4% for mass throughout the entire period (Figures 2b and d). Correlation between the total numbers, 0.6–10 μm, and those of smaller particles (<5 μm) was strong ($r > 0.999$ for number and $r = 0.990$ for mass concentration, $p < 0.001$). These results indicate that smaller particles predominate in the TB core.

Average dust concentrations in the TB core were compared with those in other ice cores from the Himalayas (Table 1). In terms of overall averages, dust number concentrations in the TB core were 11.8 and 2.1 times higher than those of the ER and DP cores, respectively, and the dust mass concentration of the TB core was 1.6 times that of the ER core (no data were available for the DP core). However, measurement periods and size ranges differed among the cores, with the ER and DP cores covering the past 14 and 5 centuries, respectively, much longer than the TB core period. For the overlapping period of 1875–1996 CE, the dust number concentration in the TB core was $(10.4 \pm 8.5) \times 10^4$ mL^{-1} while that in the DP core was $(7.2 \pm 3.6) \times 10^4$ mL^{-1}. Although the DP core covers a wider size range (0.6–20 μm), the TB core still exhibits ~1.4 times higher concentration. A Welch's t-test was conducted to compare the annual mean dust number concentrations between the two cores during this period, revealing a statistically significant difference ($t = -3.83$, $p < 0.001$). These results indicate that the mean dust number concentration in the TB core was significantly higher than that in the DP core (no dust concentration data were available for the ER core).

Wake et al. (1994) measured microparticle concentrations in snow samples from the Ngozumpa glacier on the southern slopes of the Nepal Himalayas (Figure 1b) and noted that the levels were low, with a number concentration of 5.9×10^4 mL^{-1} for the size range of 0.6–13 μm, implying minimal influence of the vast arid and semi-arid regions of Central Asia. In contrast, an ice core drilled at Mera Peak (Figure 1b), also on the southern slopes of the Himalayas, yielded much higher concentrations, with a mass concentration of 10.1×10^3 μg kg^{-1} in the size range of 1–30 μm (Ginot et al., 2014). This suggests that dust concentrations in ice cores drilled on the southern slopes of the Himalayas are likely higher than those on the northern slopes. The results of Wake et al. (1994) were based on snow samples from 1989 to 1990 CE, a very limited record, and may not fully reflect dust deposition in the region.

However, the dust mass concentration in the TB core is an order of magnitude lower than that of Tibetan ice cores. For example, the average dust mass concentration in the Mugagangqiong core of central Tibet (Figure 1b; Li et al., 2019) is 11.3 times that of the TB core. This is consistent with previous studies, which reported that the highest concentrations of dust and crustal elements (e.g., Ca^{2+}) in Tibetan ice cores occur in the northwest, near arid regions such as the Taklamakan Desert and Qaidam Basin, and decrease toward the southeast with the lowest

Journal of Geophysical Research: Atmospheres 10.1029/2025JD043492

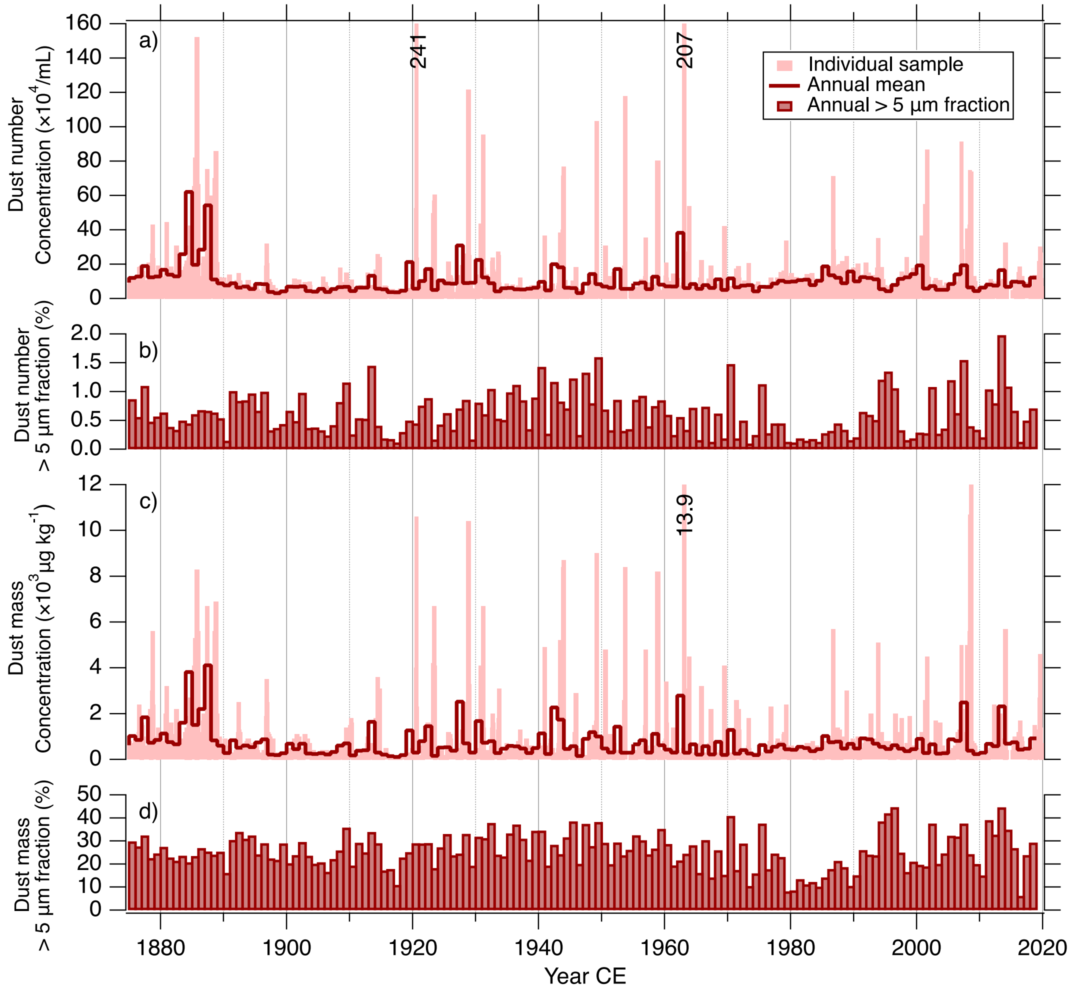

Figure 2. Dust concentrations in the Trambau core for (a) particle number and (c) mass for 1875–2019. Proportions of large particles (>5 μm) in the total concentration are presented for (b) number and (d) mass. The values indicate overshoot spikes in concentration.

concentrations in the Himalayas (Wake et al., 1993; Wu et al., 2010; W. Zhang et al., 2016; Yang et al., 2022). The TB core thus highlights the contrasting dust concentrations of the northern and southern slopes of the Himalayas.

Particle size distributions relative to dust mass and number concentrations in the TB core are shown in Figure 3. The number concentration (Figure 3a) is higher for smaller particles, decreasing logarithmically as particle size increases, consistent with the Junge distribution for continental aerosols (Junge, 1955). The size distribution relative to mass concentration is shown in Figure 3b. The average distribution over the entire period is unimodal, with a modal value of 5.0 μm.

Table 1
Comparison of Dust Concentrations From Three Himalayan Ice Cores: TB (Trambau; This Study), ER (East Rongbuk; Xu et al., 2010), and DP (Dasuopu; Thompson et al., 2000)

	Latitude (°N)	Longitude (°E)	Elevation (m a.s.l.)	Period (year CE)	Size range (μm)	Number ($\times10^4$ mL^{-1})	Mass ($\times10^3$ μg kg^{-1})
TB	27.92	86.54	5,862	1875–2019	0.6–10	10.35	0.73
ER	27.59	86.55	6,518	600–1960	1.0–30	0.88	0.47
DP	28.23	85.43	7,200	1450–1996	0.6–20	4.93	n/a

Note. n/a means not available.

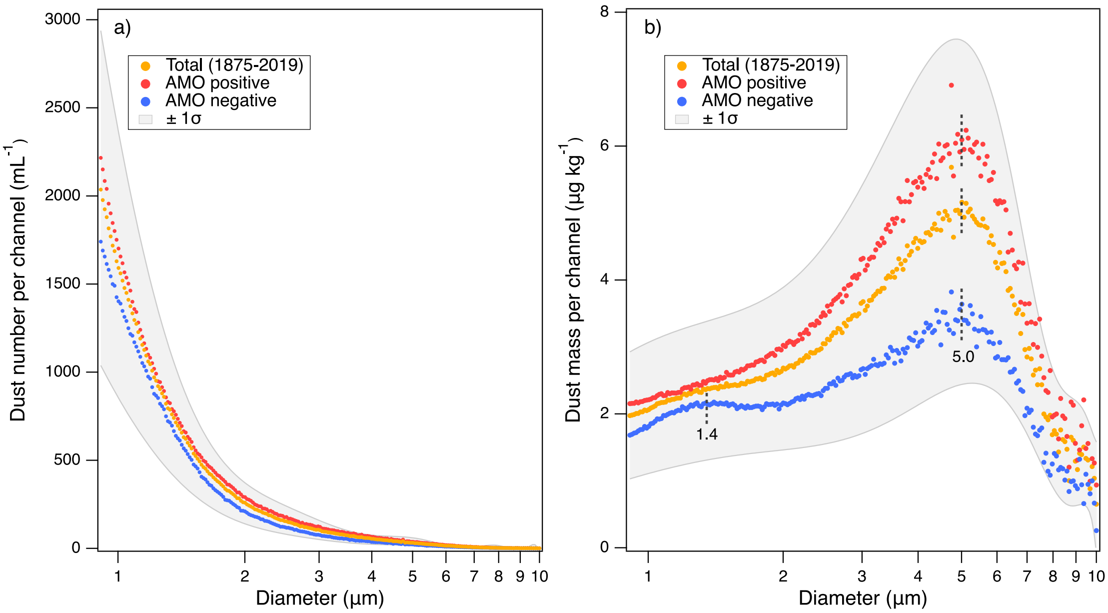

Figure 3. Dust particle size distributions in the Trambau core for (a) number and (b) mass concentration. Vertical axes represent dust concentration per measurement channel (out of 300 total channels); horizontal axes represent the logarithm of particle size diameter. Orange, red, and blue dots indicate average distributions for the entire period (1875–2019), for the Atlantic Multidecadal Oscillation (AMO) positive phase (high-concentration period: 1875–1900, 1928–1962, 1998–2019), and the AMO negative phase (low-concentration period: 1901–1927, 1963–1997), respectively. Gray shading represents ±1 standard deviation for the entire period. Values in (b) are modal values of each distribution.

The dust particle size distribution was compared with records from nearby ice cores and snow samples. The modal value for the TB core is similar to those reported for the HMA, particularly the Tien Shan Mountains and northwestern Tibet (4–7 μm; Wake et al., 1994; W. Zhang et al., 2017). In contrast, modal values reported for the northern slopes of the Himalayas are smaller than that of the TB core, with snow samples from Mt. Shishapangma Peak, near the DP site, yielding sizes of ∼3 μm (Wake et al., 1994) and the ER core 3.2–4.2 μm (Xu et al., 2010). An ice core drilled at Mera Peak (Figure 1b) yielded a mode of 5.7–6.2 μm for the period 1999–2010 CE (Ginot et al., 2014), compared with 5.3 μm calculated for the TB core for the same period. This suggests that the particle size distribution varies between the northern and southern slopes of the Himalayas, with larger average particle sizes on the southern slopes. This is likely because the southern sites are located closer to major dust sources (see Section 3.3 for details on dust sources). Although Wu et al. (2009) reported that differences in particle size distribution depend on dust concentration rather than geographical location, our results suggest that geographical location affects both north-south concentration gradient and size distribution.

Regarding the dust mass size distribution, previous studies have reported a pattern of decreasing dust concentration approaching zero for particle sizes <2 μm (Ginot et al., 2014; W. Zhang et al., 2016, 2017). In contrast, the TB core exhibits a distinct pattern whereby the concentration remains high even for particles of <2 μm size (Figure 3b). This suggests that the TB core contains a relatively high proportion of fine dust particles compared with the other cores, possibly indicating dust from more distant sources.

The modal particle sizes for the ER core differ significantly between low-concentration periods (3.2 μm for 1815–1825 CE) and high-concentration periods (4.2 μm for 1690–1730 CE) (Xu et al., 2010). In contrast, the modal values of the TB core are similar in high- and low-concentration periods (Figure 3b; e.g., 4.96 μm during the AMO positive phase, and 5.01 μm during the negative phase). However, the mass size distribution of the TB core indicates higher concentrations of smaller particles (∼1.4 μm) during the low-concentration period, with a bimodal distribution (Figure 3b). The unimodal distribution in the ER core indicates a single primary dust source in the arid regions of Central Asia (Xu et al., 2010) while multiple more distant sources may have contributed to the TB core during low-concentration periods.

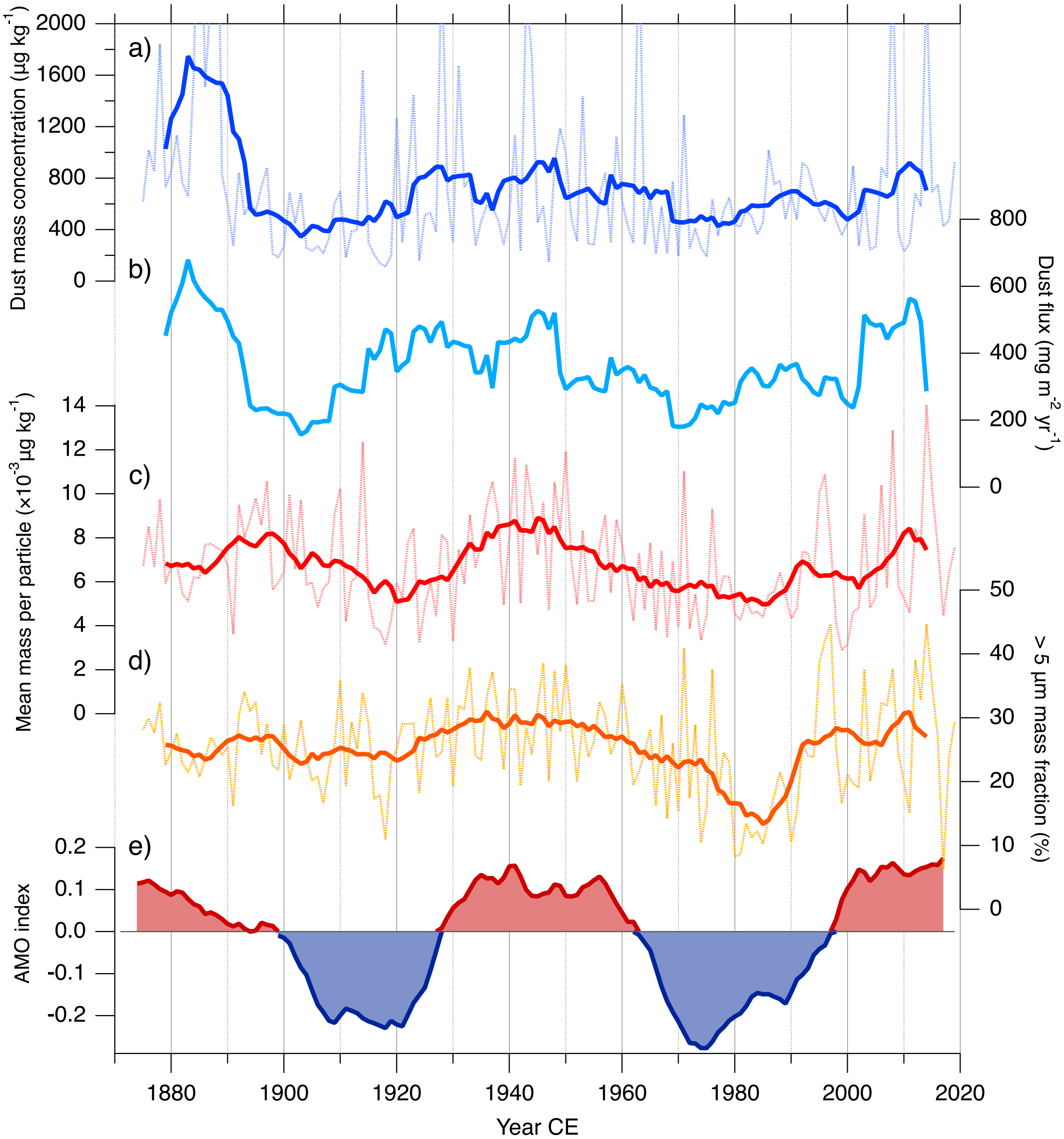

Figure 4. Time series of dust concentration, flux, particle properties in the Trambau core, and the Atlantic Multidecadal Oscillation (AMO) index for 1875–2019. (a) Dust mass concentration; (b) dust flux; (c) mean mass concentration per particle; (d) mass fraction of large particles (>5 µm); and (e) annual mean AMO index. Dashed lines in (a, c, d) represent annual averages; solid lines in (a–d) represent 11-year running averages.

3.2. Time Series of Dust Concentration

The time series of dust mass concentrations in the TB core during 1875–2019 CE is shown in Figure 4a. The dust concentration in the TB core was highest in the 1880s, and although high-concentration peaks were observed in other years (Figures 2a and 2c), the baseline concentration in the early 1880s is clearly higher than that in other periods. In contrast, the nearby ER and DP core sites do not show notable dust peaks for the 1880s (Thompson et al., 2000; Xu et al., 2010). A possible explanation for the high dust concentration in the TB core is the severe drought in India during 1876–1877 CE, which is recorded in the DP core where high dust and Cl^- concentrations are linked to a drought event caused by a weakening of the Indian summer monsoon (Thompson et al., 2000). Although no dust concentration peak occurs in the ER core during this time interval (Xu et al., 2010), other studies of the core have reported elevated Ca^{2+} concentrations in the 1880s (Qin et al., 2002) and intermittent high Fe (a proxy for mineral dust) concentrations in the late 19th century (Kaspari et al., 2009). While the dust peak in the TB core appears ~5 years after that in the DP core, and no significant Cl^- peak was found, the TB peak in the early

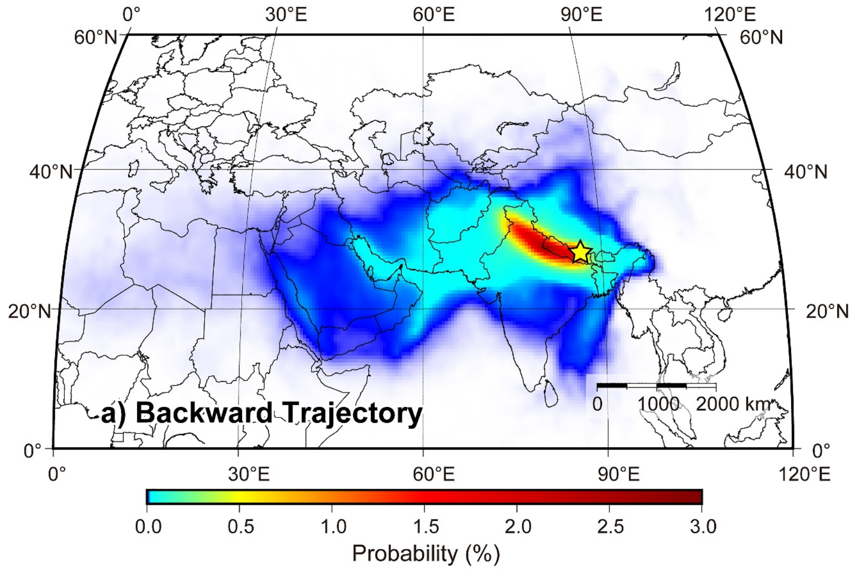

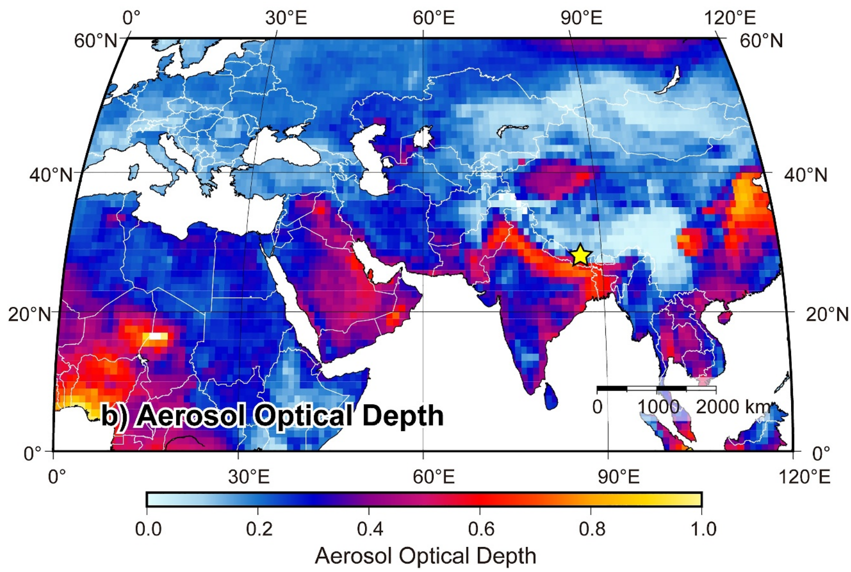

Figure 5. Distributions of (a) air mass back-trajectories and (b) Aerosol Optical Depth (AOD) over potential dust source regions for the Trambau (TB) core site (yellow star). (a) Probability distribution for an air mass arriving at the TB core site from a 10-day back-trajectory analysis during the winter-spring season (December-April) for 1960–2019. (b) Decadal mean (November 2009 to October 2019) of the Moderate Resolution Imaging Spectroradiometer-derived Aerosol Optical Depth index.

1880s may have been influenced by the Indian drought, especially considering the potential dating uncertainty in the DP core (Hou et al., 2018).

Dust concentrations in the TB core show 50- to 70-year cycles, including the high-concentration period in the 1880s (Figure 4a). The multidecadal variability in dust concentrations is discussed further in Section 3.4.

3.3. Dust Source Regions

Aerosol transport by westerlies is dominant in the Himalayas during winter and spring (Kang et al., 2004; Kaspari et al., 2009; Xu et al., 2007). High concentrations of aerosols have been reported through atmospheric observations, particularly during the pre-monsoon season (Bonasoni et al., 2010). Therefore, we constructed 10-day back-trajectories for the 5-month period December-April, using 60-year average values from 1960 to 2019 CE

Table 2
Correlation Coefficients Between the Atlantic Multidecadal Oscillation Index and Dust Properties in the Trambau Core

	Dust mass concentration	Dust flux	Mass per particle	>5 μm mass fraction
Annual	0.226[a]	0.160[b]	0.308	0.337
5 year	0.372	0.344	0.562	0.576
11 year	0.457	0.480	0.683	0.700

[a]$0.01 > p > 0.001$, [b]$p > 0.05$, no remark $p < 0.001$.

(Figure 5a). The trajectories overlapped distant arid regions including the Arabian Peninsula and Southwest Asia (specifically Iran, Afghanistan, and Pakistan), as well as relatively proximal areas such as the Thar Desert in northwest India (Figure 1a).

To capture the dust aerosol loading in the atmosphere around the TB site, we studied the decadal average AOD for the period November 2009 to October 2019 (10 years prior to core drilling) (Figure 5b). The spatial distribution of AOD revealed a band of high aerosol loading along the southern side of the Himalayas, indicating that dust from Southwest Asia, including the Thar Desert, was transported eastward along this side of the range. The Himalayas likely act as a barrier to the northward transport of dust, with less deposition in the northern region. This distribution supports the contrasting dust concentrations between ice core sites on the northern and southern slopes. To visualize the spatial distribution of atmospheric dust load over the HMA region, satellite-derived data such as MODIS AOD have been used in several studies (e.g., Wu et al., 2010). However, AOD data do not exclusively represent dust load, as they also reflect the presence of other aerosols. Therefore, caution should be taken when interpreting the implications of the AOD data.

Back-trajectory analyses have also been undertaken for the ER core, showing a similar distribution of trajectories, but with each study identifying different source regions based on additional analyses. Based on the unimodal dust size distribution of the ER core, Xu et al. (2010) concluded that the extensive arid and semi-arid regions of Central Asia were the only primary source area. Kaspari et al. (2009) identified primary sources as the Arabian Peninsula, Thar Desert, and northern Sahara Desert based on spatial correlation between a satellite-based aerosol index and Fe concentrations in the ER core. Xu et al. (2009) used Sr-Nd-Pb analyses to clarify the dust composition and concluded that the main sources lay in Northwest India including the Thar Desert, excluding the Sahara and Taklamakan deserts. Primary dust sources for the TB core are presumed to be the Middle East, Southwest Asia, and the Thar Desert, consistent with source areas for the ER core. There appear to be no significant differences in back-trajectory air mass distributions between the ER and TB core sites. It follows that differences in concentration and particle size between the two sites are not due to differences in sources but are more likely due to differences in air mass transport, with the Himalayan range acting as a barrier for the ER core site (Wake et al., 1994; Wu et al., 2010).

3.4. Multidecadal Variability of Dust and the AMO

Dust records from ice cores are often compared with climate indices, as dust concentration and particle size reflect atmospheric conditions. HMA ice-core dust records have shown significant correlations with the NAO (Xu et al., 2007; Y. Zhang et al., 2015; W. Zhang et al., 2017). However, the dust mass concentration in the TB core shows no significant correlation with the NAO ($r = -0.11$, $p > 0.05$) for the period 1875–2015 CE; rather, 50- to 70-year cycles are evident (Figure 4a). The mean mass per particle (mass concentration/number concentration) and the mass fraction of large (>5 μm) particles in the total concentration similarly display 50- to 70-year variations (Figures 4c and 4d). These variations correspond to AMO phases (Figure 4e), with higher values for these dust properties observed during positive AMO phases and vice versa. For the TB core, annual means of dust mass concentration, mass per particle, and the >5 μm mass fraction are significantly correlated with the AMO ($r = 0.23$–0.34; Table 2). However, the dust number concentration in the DP core is not correlated with the AMO ($r = 0.05$, $p > 0.05$, 1875–1996 CE; Thompson et al., 2000). To assess the significance of the multidecadal variability in the dust data, we performed spectral analysis using the Lomb-Scargle periodogram with a red-noise background estimation analogous to the REDFIT method (Schulz & Mudelsee, 2002). The TB core dust mass concentration exhibited a statistically significant periodicity at the 95% confidence level, comparable to that observed in the AMO. In contrast, the multidecadal variability in the DP core dust number concentration was not statistically significant.

Dust concentrations in ice cores may be influenced by local snow accumulation at the drilling site, which might be affected by AMO. To investigate the factors underlying the observed relationship between dust concentrations in the TB core and AMO, we compared the TB dust record with annual accumulation rates reconstructed from annual layer thicknesses dated by Tsushima et al. (2025). It should be noted that the TB drilling site is affected by glacier flow and melt-refreeze processes, and the accumulation rates used here are provisional, as they have not been corrected for these influences (therefore figure is not shown). A negative correlation was found between the annual accumulation and AMO ($r = -0.31$, $p < 0.001$), suggesting that periods of negative AMO tend to coincide with higher accumulation rates. This implies that during the negative AMO phases, increased accumulation could dilute the dust content in snow, leading to lower dust concentrations and vice versa. Therefore, the observed positive correlation between dust concentration and AMO might be influenced by changes in accumulation. To evaluate the potential impact of accumulation, we calculated dust flux by multiplying dust mass concentration by accumulation and compared it with the other variables (Figure 4b and Table 2). The dust flux also shows a positive correlation with AMO ($r = 0.48$), comparable to that between AMO and the dust mass concentration ($r = 0.46$). In contrast, the dust flux shows no significant correlation with the accumulation ($r = 0.08$, $p > 0.05$), whereas it strongly correlates with the dust concentration ($r = 0.81$, $p < 0.001$). These results suggest that the relationship between AMO and dust concentration in the TB core primarily reflects changes in dust deposition and that the influence of accumulation at the drilling site is likely limited.

To explore these relationships further, we analyzed the spatial distribution of the correlation of the ERA5 reanalysis data and the PDSI during the winter-spring season (December-April) during 1941–2019 CE, with both the dust mass concentration in the TB core and the AMO (Figure 6). For potential dust source regions of the Middle East and Southwest Asia, we found that dust concentrations are positively correlated with temperature, with patchy negative correlations with precipitation and PDSI (Figures 6a–6c). The spatial distributions of correlations with the AMO show similar but clearer patterns (Figures 6d–6f). These observations suggest that during periods of high dust concentration, potential dust source regions are characterized by higher temperatures, less precipitation, and more negative PDSI values, and vice versa.

We further undertook composite analyses to investigate the degree of fluctuation in the variables that occur independently of the degree of correlation (Figure 7). Particularly in the Middle East and Southwest Asia, precipitation and PDSI values indicate drier conditions during positive AMO phases, and vice versa (Figures 7b, 7c, 7f, and 7g). For temperature (Figures 7a and 7e), the high-temperature tendency during positive AMO phases may have enhanced drier conditions. However, as the 5 years with the highest positive AMO phases occurred in the 2000s, and those with the most negative phases occurred in the 1970s, this pattern may simply reflect a broader warming trend. To determine whether this is attributable to the AMO, temperature data must be detrended by removing the linear trend. We examined wind speed and direction at the 500 hPa level, which is relevant for aerosol transport at the elevation of the ice core site, and found that westerly winds toward the TB site were enhanced during both positive and negative AMO phases (Figures 7d and 7h). However, there are no clear differences that would affect the dust supply. Furthermore, the same composite analysis for the back-trajectory distributions suggests no significant differences in the trajectory patterns (figure not shown). These results suggest that dust concentrations in the TB core are more strongly influenced by changes in source-region surface conditions than by variations in atmospheric circulation.

We found positive correlations between the AMO and the dust mass concentration, dust flux, mean mass per particle, and large-particle mass fraction (Figure 4; Table 2). This suggests a lower contribution of larger particles and reduced overall particle size during negative AMO phases. Indeed, the dust mass size distribution shows a secondary peak at ~1.4 μm during negative AMO phases, resulting in a bimodal distribution (Figure 3b). Wetter surface conditions in primary dust source regions would have suppressed dust emissions, with dust then being sourced predominantly from more distant regions.

It is thus clear that dust concentrations in the TB core were strongly influenced by the AMO, while the DP core, on the northern slopes, was less affected. This may be explained by only a small fraction of air masses passing over AMO-influenced dust source regions reaching the northern slopes. The spatial distribution of AOD (Figure 5b) shows a clear contrast in aerosol concentration between the southern and northern sides of the Himalayas. Air masses carrying dust from regions that have become drier under the influence of the AMO are blocked by the

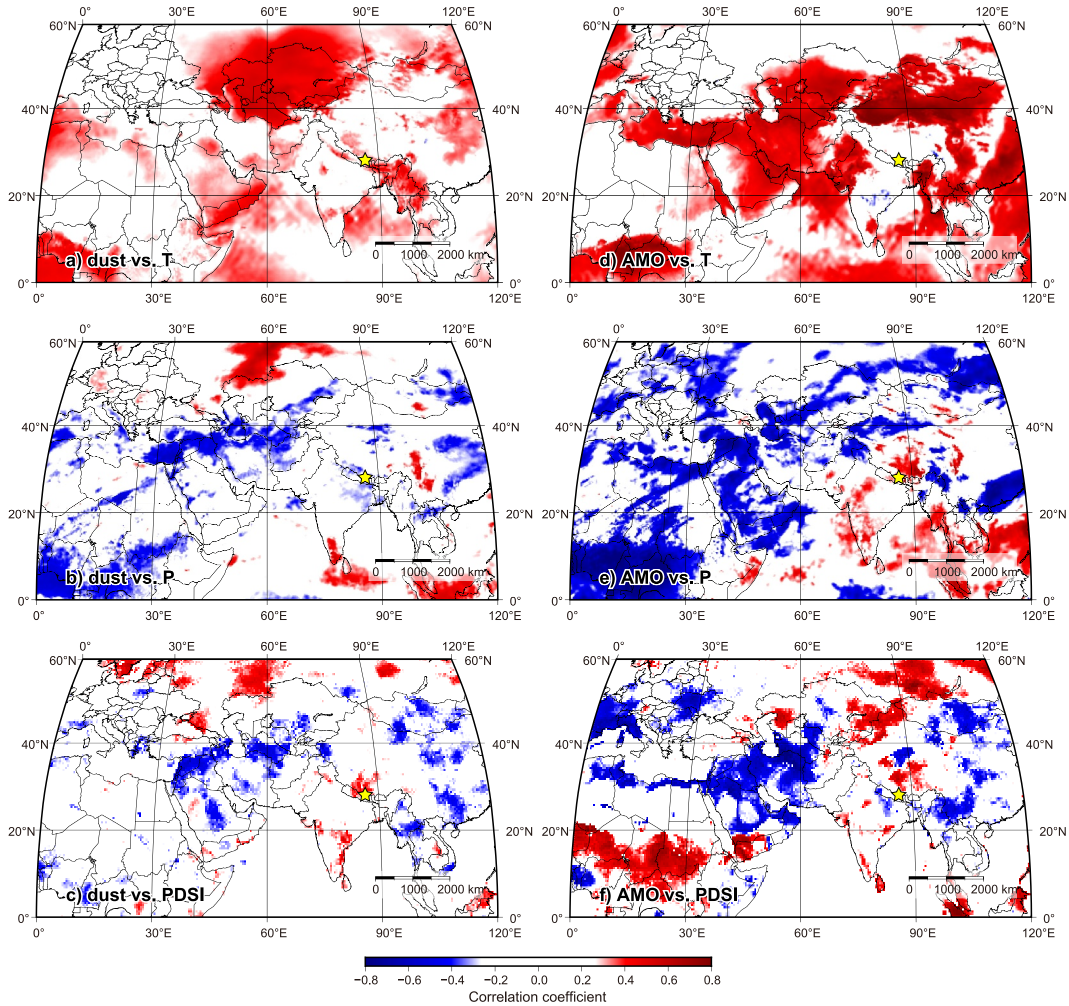

Figure 6. Spatial correlation between the ERA5 reanalysis (a and d) surface air temperature and (b and e) precipitation, and (c and f) Palmer Drought Severity Index for the winter-spring season (December-April) with (a–c) dust mass concentration in the TB core and (d–f) the Atlantic Multidecadal Oscillation index (1941–2019). The color scale indicates correlation coefficients based on 5-year running averages.

Himalayan barrier, with few reaching the northern side. Therefore, dust concentrations on the southern side of the Himalayas are dominated by the AMO, while those on the northern side are less affected, and perhaps more affected by other climate indices such as the NAO.

Previous studies have also shown that changes in precipitation associated with positive and negative AMO phases affect surface conditions, thereby influencing dust loading. For example, the negative-positive AMO transition during 1980–2006 led to increased precipitation in the Sahel region of West Africa. This, in turn, reduced dust concentrations in downwind marine areas (Foltz & McPhaden, 2008; Wang et al., 2012). This relationship, however, is opposite to that recorded in the TB core. Although direct mechanisms that AMO influences the climate conditions of the Middle East and Southwest Asia remain unclear, multidecadal variations in temperature and precipitation, such as those observed in the Sahel region, could occur in the regions. Compared with regions such as Europe and North America, long-term observational data from the Middle East and Southwest Asia are limited, particularly during periods when the AMO phase was negative in the 1980s. As a result, direct observational data for comparisons across positive and negative AMO phases are scarce. Establishing more observation sites and continuing long-term monitoring over the coming decades may help to clarify the mechanisms linking AMO variability to climate conditions in the regions. On a broader scale, satellite observations have revealed a decreasing trend in global and North African dust concentrations since 1975 (Shao et al., 2013), contradicting the trend revealed by the TB core. Although satellite observations and model simulations have

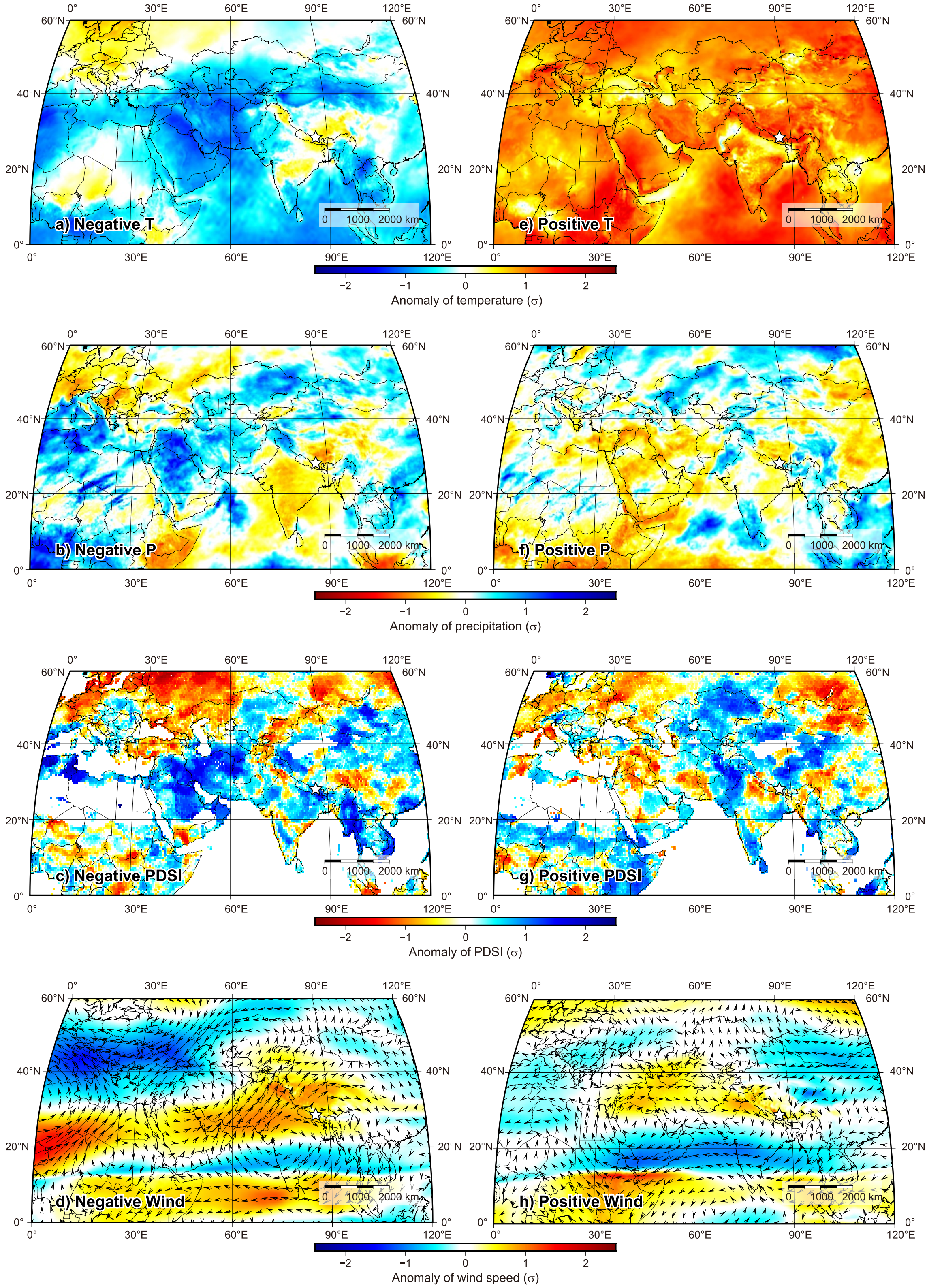

Figure 7. Composite analyses for the ERA5 reanalysis (a and e) surface air temperature, (b and f) precipitation, (c and g) Palmer Drought Severity Index, and (d and h) 500 hPa wind speed and direction (vectors) for the winter-spring season (December-April). Five-year composites are made with (left panels, a–d) the most negative Atlantic Multidecadal Oscillation (AMO) (1972, 1973, 1974, 1975, 1976) and (right panels, e–h) the most positive AMO (2008, 2009, 2015, 2016, 2017), respectively. Color scales represent anomalies expressed in terms of the standard deviation (σ). White stars indicate the location of the Trambau core site.

enhanced our understanding of the global distribution and variability of dust concentrations, regions with sparse observational data, such as the Himalayas, still exhibit significant uncertainties (Ginoux et al., 2012; Mahowald et al., 2010). Our TB dust data offer valuable new constraints for model simulations, providing critical insights that may reduce uncertainties in such understudied regions.

4. Conclusions

This study presents a 145-year atmospheric dust record reconstructed from the TB ice core drilled on the southern slopes of the Himalayas—a region for which, to our knowledge, there were no previous long-term dust records. This record enabled a comparison between ice cores from both sides of the Himalayan range, showing that the TB core contains higher dust concentrations than the ER and DP cores from the northern slopes. The southern slopes are strongly influenced by the AMO, and the northern slopes are less so, likely due to the Himalayan range acting as a barrier to air mass transport. Our results for the TB core indicate that even for ice cores drilled in geographically proximal locations within the same Himalayan range, there are significant differences between the southern and northern slopes, confirming that no single ice core can fully represent the entire Himalayan region. Given current data limitations, the identification of the factors behind these variations remains challenging. Additional ice core drilling and data comparisons are essential to advance our understanding of atmospheric conditions in the Himalayan region.

Data Availability Statement

Dust and age scale data for the TB core are available from Zenodo (Esashi, 2025; Tsushima & Fujita, 2024). Dust data for the DP core are archived at the National Centers for Environmental Information (NCEI), National Oceanic and Atmospheric Administration (NOAA) (Thompson et al., 2000; https://www.ncei.noaa.gov/access/paleo-search/study/11180). ERA5 monthly averaged data on single levels were obtained from the Copernicus Climate Data Store (Hersbach et al., 2020; https://cds.climate.copernicus.eu/). The AMO index (Enfield et al., 2001; https://www.psl.noaa.gov/data/timeseries/AMO/) and the NAO index based on the 20CRV3 dataset (Compo et al., 2011; https://psl.noaa.gov/data/20thC_Rean/timeseries/monthly/NAO/) were obtained from the NOAA Physical Sciences Laboratory. Palmer Drought Severity Index data (1901–2022 Preliminary 4.07) were obtained from the Climatic Research Unit (CRU) at the University of East Anglia (van der Schrier et al., 2013; Barichivich et al., 2022; https://crudata.uea.ac.uk/cru/data/drought/). MODIS Aqua AOD data (Aerosol Optical Depth at 550 nm, Deep Blue, Land-only, MYD08_M3 v6.1) were accessed via NASA's Giovanni data portal (Platnick et al., 2015; https://giovanni.gsfc.nasa.gov/giovanni/).

Acknowledgments

The authors would thank members of the 2019 drilling team. The authors also appreciate K. Kawakami, T. Saito, A. Watari, and M. Otsuka for supporting the ice core processing in the cold rooms of the Institute of Low Temperature Science, Hokkaido University, Japan. This study is supported by JSPS-KAKENHI (Grants 17H01621, 18H05292, 22H00033, 23H00511, and 23KJ1076), the Grant for Joint Research Program of the Institute of Low Temperature Science, Hokkaido University (Grants 20G047, 21G034, 22G029, and 23G053), and the Nagoya University Interdisciplinary Frontier Fellowship supported by JST and Nagoya University.

References

Barichivich, J., Osborn, T. J., Harris, I., van der Schrier, G., & Jones, P. D. (2022). Monitoring global drought using the self-calibrating Palmer drought Severity index [in "state of the climate in 2021"]. *Bulletin of the American Meteorological Society*, *103*(8), S66–S67. https://doi.org/10.1175/BAMS-D-22-0092.1

Birkel, S. D., Mayewski, P. A., Maasch, K. A., Kurbatov, A. V., & Lyon, B. (2018). Evidence for a volcanic underpinning of the Atlantic multidecadal oscillation. *Npj Climate and Atmospheric Science*, *1*(1), 1–7. https://doi.org/10.1038/s41612-018-0036-6

Bonasoni, P., Laj, P., Marinoni, A., Sprenger, M., Angelini, F., Arduini, J., et al. (2010). Atmospheric Brown Clouds in the Himalayas: First two years of continuous observations at the Nepal climate Observatory-Pyramid (5079 m). *Atmospheric Chemistry and Physics*, *10*(15), 7515–7531. https://doi.org/10.5194/acp-10-7515-2010

Booth, B. B. B., Dunstone, N. J., Halloran, P. R., Andrews, T., & Bellouin, N. (2012). Aerosols implicated as a prime driver of twentieth-century North Atlantic climate variability. *Nature*, *484*(7393), 228–232. https://doi.org/10.1038/nature10946

Compo, G. P., Whitaker, J. S., Sardeshmukh, P. D., Matsui, N., Allan, R. J., Yin, X., et al. (2011). The twentieth century reanalysis project. *Quarterly Journal of the Royal Meteorological Society*, *137*(654), 1–28. https://doi.org/10.1002/qj.776

Cristofanelli, P., Bracci, A., Sprenger, M., Marinoni, A., Bonafè, U., Calzolari, F., et al. (2010). Tropospheric ozone variations at the Nepal Climate Observatory-Pyramid (Himalayas, 5079 m a.s.l.) and influence of deep stratospheric intrusion events. *Atmospheric Chemistry and Physics*, *10*(14), 6537–6549. https://doi.org/10.5194/acp-10-6537-2010

Dai, A., Trenberth, K. E., & Qian, T. (2004). A global dataset of Palmer drought Severity index for 1870–2002: Relationship with soil Moisture and effects of surface warming. *Journal of Hydrometeorology*, *5*(6), 1117–1130. https://doi.org/10.1175/JHM-386.1

Delmonte, B., Petit, J., & Maggi, V. (2002). Glacial to Holocene implications of the new 27000-year dust record from the EPICA Dome C (East Antarctica) ice core. *Climate Dynamics*, *18*(8), 647–660. https://doi.org/10.1007/s00382-001-0193-9

Delworth, T. L., & Mann, M. E. (2000). Observed and simulated multidecadal variability in the Northern Hemisphere. *Climate Dynamics*, *16*(9), 661–676. https://doi.org/10.1007/s003820000075

Enfield, D. B., Mestas-Nuñez, A. M., & Trimble, P. J. (2001). The Atlantic Multidecadal Oscillation and its relation to rainfall and river flows in the continental U.S. *Geophysical Research Letters*, *28*(10), 2077–2080. https://doi.org/10.1029/2000gl012745

Esashi, N. (2025). Dust concentrations in Trambau ice core, Nepal Himalaya [Dataset]. *Zenodo*. https://doi.org/10.5281/zenodo.14728819

Foltz, G. R., & McPhaden, M. J. (2008). Trends in Saharan dust and tropical Atlantic climate during 1980–2006. *Geophysical Research Letters*, *35*(20), L20706. https://doi.org/10.1029/2008GL035042

Ginot, P., Dumont, M., Lim, S., Patris, N., Taupin, J.-D., Wagnon, P., et al. (2014). A 10 year record of black carbon and dust from a Mera peak ice core (Nepal): Variability and potential impact on melting of Himalayan glaciers. *The Cryosphere*, *8*(4), 1479–1496. https://doi.org/10.5194/tc-8-1479-2014

Ginoux, P., Prospero, J. M., Gill, T. E., Hsu, N. C., & Zhao, M. (2012). Global-scale attribution of anthropogenic and natural dust sources and their emission rates based on MODIS Deep Blue aerosol products. *Reviews of Geophysics*, *50*(3), RG3005. https://doi.org/10.1029/2012rg000388

Griffin, D., & Kellogg, C. (2004). Dust storms and their impact on ocean and human health: Dust in Earth's atmosphere reviews. *EcoHealth*, *1*(3), 284–295. https://doi.org/10.1007/s10393-004-0120-8

Hersbach, H., Bell, B., Berrisford, P., Hirahara, S., Horányi, A., Muñoz-Sabater, J., et al. (2020). The ERA5 global reanalysis. *Quarterly Journal of the Royal Meteorological Society*, *146*(730), 1999–2049. https://doi.org/10.1002/qj.3803

Hou, S., Jenk, T. M., Zhang, W., Wang, C., Wu, S., Wang, Y., et al. (2018). Age ranges of the Tibetan ice cores with emphasis on the Chongce ice cores, western Kunlun Mountains. *The Cryosphere*, *12*(7), 2341–2348. https://doi.org/10.5194/tc-12-2341-2018

Iizuka, Y., Uemura, R., Fujita, K., Hattori, S., Seki, O., Miyamoto, C., et al. (2018). A 60 year record of atmospheric aerosol depositions preserved in a high-accumulation dome ice core, southeast Greenland. *Journal of Geophysical Research: Atmospheres*, *123*(1), 574–589. https://doi.org/10.1002/2017JD026733

Ji, Z., Kang, S., Zhang, Q., Cong, Z., Chen, P., & Sillanpää, M. (2016). Investigation of mineral aerosols' radiative effects over High Mountain Asia in 1990–2009 using a regional climate model. *Atmospheric Research*, *178–179*, 484–496. https://doi.org/10.1016/j.atmosres.2016.05.003

Jickells, T. D., An, Z. S., Andersen, K. K., Baker, A. R., Bergametti, G., Brooks, N., et al. (2005). Global iron connections between desert dust, ocean biogeochemistry, and climate. *Science*, *308*(5718), 67–71. https://doi.org/10.1126/science.1105959

Junge, C. (1955). The size distribution and aging of natural aerosols as determined from electrical and optical data on the atmosphere. *Journal of Meteorology*, *12*(1), 13–25. https://doi.org/10.1175/1520-0469(1955)012<0013:TSDAAO>2.0.CO;2

Kang, S., Mayewski, P. A., Qin, D., Sneed, S. A., Ren, J., & Zhang, D. (2004). Seasonal differences in snow chemistry from the vicinity of Mt. Everest, central Himalayas. *Atmospheric Environment*, *38*(18), 2819–2829. https://doi.org/10.1016/j.atmosenv.2004.02.043

Kang, S., Mayewski, P. A., Qin, D., Yan, Y., Hou, S., Zhang, D., et al. (2002). Glaciochemical records from a Mt. Everest ice core: Relationship to atmospheric circulation over Asia. *Atmospheric Environment*, *36*(21), 3351–3361. https://doi.org/10.1016/S1352-2310(02)00325-4

Kaspari, S., Mayewski, P. A., Handley, M., Kang, S., Hou, S., Sneed, S., et al. (2009). A high-resolution record of atmospheric dust composition and variability since AD 1650 from a Mount Everest ice core. *Journal of Climate*, *22*(14), 3910–3925. https://doi.org/10.1175/2009JCLI2518.1

Kaspari, S., Mayewski, P. A., Kang, S., Sneed, S., Hou, S., Hooke, R., et al. (2007). Reduction in northward incursions of the South Asian monsoon since ∼1400 AD inferred from a Mt. Everest ice core. *Geophysical Research Letters*, *34*(16), L16701. https://doi.org/10.1029/2007GL030440

Li, P., Wu, G., Zhang, X., Yan, N., & Zhang, X. (2019). Variation in atmospheric dust since 1950 from an ice core in the central Tibetan Plateau and its relationship to atmospheric circulation. *Atmospheric Research*, *220*, 10–19. https://doi.org/10.1016/j.atmosres.2018.12.030

Luterbacher, J., Xoplaki, E., Dietrich, D., Jones, P. D., Davies, T. D., Portis, D., et al. (2001). Extending North Atlantic oscillation reconstructions back to 1500. *Atmospheric Science Letters*, *2*(1–4), 114–124. https://doi.org/10.1006/asle.2002.0047

Mahowald, N. M., Kloster, S., Engelstaedter, S., Moore, J. K., Mukhopadhyay, S., McConnell, J. R., et al. (2010). Observed 20th century desert dust variability: Impact on climate and biogeochemistry. *Atmospheric Chemistry and Physics*, *10*(22), 10875–10893. https://doi.org/10.5194/acp-10-10875-2010

Miller, R. L., & Tegen, I. (1998). Climate response to soil dust aerosols. *Journal of Climate*, *11*(12), 3247–3267. https://doi.org/10.1175/1520-0442(1998)011<3247:CRTSDA>2.0.CO;2

Ortega, P., Lehner, F., Swingedouw, D., Masson-Delmotte, V., Raible, C. C., Casado, M., & Yiou, P. (2015). A model-tested North Atlantic Oscillation reconstruction for the past millennium. *Nature*, *523*(7558), 71–74. https://doi.org/10.1038/nature14518

Palmer, W. C. (1965). *Meteorological drought. Office of Climatology Research Paper No. 45*. U.S. Weather Bureau. Retrieved from https://www.droughtmanagement.info/literature/USWB_Meteorological_Drought_1965.pdf

Parvin, F., Seki, O., Fujita, K., Iizuka, Y., Matoba, S., Ando, T., & Sawada, K. (2019). Assessment for paleoclimatic utility of biomass burning tracers in SE-Dome ice core, Greenland. *Atmospheric Environment*, *196*, 86–94. https://doi.org/10.1016/j.atmosenv.2018.10.012

Platnick, S., Hubanks, P., Meyer, K., & King, M. D. (2015). MODIS atmosphere L3 monthly product (08_L3) [Dataset]. *NASA MODIS Adaptive Processing System, Goddard Space Flight Center*. https://doi.org/10.5067/MODIS/MYD08_M3.006

Prasad, A. K., & Singh, R. P. (2007). Changes in aerosol parameters during major dust storm events (2001–2005) over the Indo-Gangetic Plains using AERONET and MODIS data. *Journal of Geophysical Research*, *112*(D9), D09208. https://doi.org/10.1029/2006JD007778

Prospero, J. M., Ginoux, P., Torres, O., Nicholson, S. E., & Gill, T. E. (2002). Environmental characterization of global sources of atmospheric soil dust identified with the Nimbus 7 Total Ozone Mapping Spectrometer (TOMS) absorbing aerosol product. *Reviews of Geophysics (1985)*, *40*(1), 2-1–2-31. https://doi.org/10.1029/2000RG000095

Qin, D., Hou, S., Zhang, D., Ren, J., Kang, S., Mayewski, P. A., & Wake, C. P. (2002). Preliminary results from the chemical records of an 80.4 m ice core recovered from East Rongbuk glacier, Qomolangma (mount Everest), Himalaya. *Annals of Glaciology*, *35*, 278–284. https://doi.org/10.3189/172756402781816799

Rosenfeld, D., Rudich, Y., & Lahav, R. (2001). Desert dust suppressing precipitation: A possible desertification feedback loop. *Proceedings of the National Academy of Sciences of the United States of America*, *98*(11), 5975–5980. https://doi.org/10.1073/pnas.101122798

Schulz, M., & Mudelsee, M. (2002). Redfit: Estimating red-noise spectra directly from unevenly spaced paleoclimatic time series. *Computers & Geosciences*, *28*(3), 421–426. https://doi.org/10.1016/S0098-3004(01)00044-9

Shao, Y., Klose, M., & Wyrwoll, K.-H. (2013). Recent global dust trend and connections to climate forcing. *Journal of Geophysical Research: Atmospheres*, *118*(19), 11107–11118. https://doi.org/10.1002/jgrd.50836

Stein, A. F., Draxler, R. R., Rolph, G. D., Cohen, M. D., & Ngan, F. (2015). NOAA's HYSPLIT atmospheric transport and dispersion modeling system. *Bulletin of the American Meteorological Society*, *96*(12), 2059–2077. https://doi.org/10.1175/BAMS-D-14-00110.1

Sunako, S., Fujita, K., Sakai, A., & Kayastha, R. B. (2019). Mass balance of Trambau Glacier, Rolwaling region, Nepal Himalaya: In-situ observations, long-term reconstruction and mass-balance sensitivity. *Journal of Glaciology*, *65*(252), 605–616. https://doi.org/10.1017/jog.2019.37

Thompson, L. G., Mosley-Thompson, E., Davis, M. E., Bolzan, J. F., Dai, J., Klein, L., et al. (1989). Holocene-late Pleistocene climatic ice core records from Qinghai-Tibetan Plateau. *Science*, *246*(4929), 474–477. https://doi.org/10.1126/science.246.4929.474

Thompson, L. G., Yao, T., Mosley-Thompson, E., Davis, M. E., Henderson, K. A., & Lin, P. (2000). A high-resolution millennial record of the South Asian monsoon from Himalayan ice cores. *Science*, *289*(5486), 1916–1920. https://doi.org/10.1126/science.289.5486.1916

Tsushima, A., Esashi, N., Matoba, S., Iizuka, Y., Uemura, R., Adachi, K., et al. (2025). Contrasting responses of ion concentration variations to atmospheric patterns in central Himalayan ice cores. *Journal of Geophysical Research: Atmospheres*, *130*(2), e2024JD042392. https://doi.org/10.1029/2024JD042392

Tsushima, A., & Fujita, K. (2024). Major ions in Trambau ice core, Nepal Himalaya [Dataset]. *Zenodo*. https://doi.org/10.5281/zenodo.14252245

Tsushima, A., Miyahara, M., Yamasaki, T., Esashi, N., Sato, Y., Kayastha, R. B., et al. (2021). Ice core drilling on a high-elevation accumulation zone of Trambau Glacier in the Nepal Himalaya. *Annals of Glaciology*, *62*(85–86), 353–359. https://doi.org/10.1017/aog.2021.15

van der Schrier, G., Barichivich, J., Briffa, K. R., & Jones, P. D. (2013). A scPDSI-based global data set of dry and wet spells for 1901–2009. *Journal of Geophysical Research: Atmospheres*, *118*(10), 4025–4048. https://doi.org/10.1002/jgrd.50355

Wake, C. P., Mayewski, P. A., Li, Z., Han, J., & Qin, D. (1994). Modern eolian dust deposition in central Asia. *Tellus Series B Chemical and Physical Meteorology*, *46*(3), 220–233. https://doi.org/10.3402/tellusb.v46i3.15793

Wake, C. P., Mayewski, P. A., Xie, Z., Wang, P., & Li, Z. (1993). Regional distribution of monsoon and desert dust signals recorded in Asian glaciers. *Geophysical Research Letters*, *20*(14), 1411–1414. https://doi.org/10.1029/93GL01682

Wang, C., Dong, S., Evan, A. T., Foltz, G. R., & Lee, S.-K. (2012). Multidecadal covariability of North Atlantic sea surface temperature, African dust, Sahel rainfall, and Atlantic hurricanes. *Journal of Climate*, *25*(15), 5404–5415. https://doi.org/10.1175/JCLI-D-11-00413.1

Wu, G., Yao, T., Xu, B., Tian, L., Zhang, C., & Zhang, X. (2009). Volume-size distribution of microparticles in ice cores from the Tibetan Plateau. *Journal of Glaciology*, *55*(193), 859–868. https://doi.org/10.3189/002214309790152492

Wu, G., Yao, T., Xu, B., Tian, L., Zhang, C., & Zhang, X. (2010). Dust concentration and flux in ice cores from the Tibetan Plateau over the past few decades. *Tellus Series B Chemical and Physical Meteorology*, *62*(3), 197–206. https://doi.org/10.1111/j.1600-0889.2010.00457.x

Xu, J., Hou, S., Chen, F., Ren, J., & Qin, D. (2009). Tracing the sources of particles in the East Rongbuk ice core from Mt. Qomolangma. *Chinese Science Bulletin*, *54*(10), 1781–1785. https://doi.org/10.1007/s11434-009-0050-5

Xu, J., Hou, S., Qin, D., Kang, S., Ren, J., & Ming, J. (2007). Dust storm activity over the Tibetan Plateau recorded by a shallow ice core from the north slope of Mt. Qomolangma (Everest), Tibet-Himal region. *Geophysical Research Letters*, *34*(17), L17504. https://doi.org/10.1029/2007GL030853

Xu, J., Hou, S., Qin, D., Kaspari, S., Mayewski, P. A., Petit, J. R., et al. (2010). A 108.83-m ice-core record of atmospheric dust deposition at Mt. Qomolangma (Everest), central Himalaya. *Quaternary Research*, *73*(1), 33–38. https://doi.org/10.1016/j.yqres.2009.09.005

Yang, D., Yao, T., Wu, G., Zhu, M., Zhao, H., Deji, et al. (2022). Different patterns and origins between northwestern and southeastern Tibetan ice core glaciochemical records over the past century. *The Science of the Total Environment*, *819*, 153195. https://doi.org/10.1016/j.scitotenv.2022.153195

Yu, R., & Zhou, T. (2004). Impacts of winter-NAO on March cooling trends over subtropical Eurasia continent in the recent half century. *Geophysical Research Letters*, *31*(12), L12204. https://doi.org/10.1029/2004GL019814

Zhang, W., Hou, S., An, W., Zhou, L., & Pang, H. (2016). Variations in atmospheric dust loading since AD 1951 recorded in an ice core from the northern Tibetan Plateau. *Annals of Glaciology*, *57*(71), 258–264. https://doi.org/10.3189/2016AoG71A559

Zhang, W., Hou, S., Liu, Y., Wu, S., An, W., Pang, H., & Wang, C. (2017). A high-resolution atmospheric dust record for 1810–2004 AD derived from an ice core in eastern Tien Shan, central Asia. *Journal of Geophysical Research: Atmospheres*, *122*(14), 7505–7518. https://doi.org/10.1002/2017JD026699

Zhang, Y., Kang, S., Zhang, Q., Grigholm, B., Kaspari, S., You, Q., et al. (2015). A 500 year atmospheric dust deposition retrieved from a Mt. Geladaindong ice core in the central Tibetan Plateau. *Atmospheric Research*, *166*, 1–9. https://doi.org/10.1016/j.atmosres.2015.06.007